PHYSICAL REVIEW E **76**, 066707 (2007)

Lattice Boltzmann method for weakly ionized isothermal plasmas

Huayu Li and Hyungson Ki*
Department of Mechanical Engineering, Michigan State University, East Lansing, Michigan 48824-1226, USA
(Received 26 February 2007; revised manuscript received 12 October 2007; published 21 December 2007)

In this paper, a lattice Boltzmann method (LBM) for weakly ionized isothermal plasmas is presented by introducing a rescaling scheme for the Boltzmann transport equation. Without using this rescaling, we found that the nondimensional relaxation time used in the LBM is too large and the LBM does not produce physically realistic results. The developed model was applied to the electrostatic wave problem and the diffusion process of singly ionized helium plasmas with a 1–3% degree of ionization under an electric field. The obtained results agree well with theoretical values.

DOI: 10.1103/PhysRevE.76.066707 PACS number(s): 02.70.−c, 52.65.−y, 52.25.Dg

I. INTRODUCTION

As the governing equation for all transport phenomena of plasmas, the Boltzmann transport equation describes the evolution of the distribution function of each species of particles in the plasma. All macroscopic variables of the plasma, such as number density and macroscopic velocity, can be retrieved through proper moments of the distribution function. Less than two decades ago, lattice Boltzmann method (LBM) emerged as an alternative method to simulate fluids flows [1]. LBM first originated from its Boolean counterpart, the lattice gas automata (LGA), but it has been proved that it can be derived directly from the continuous Boltzmann equation by discretization in both time and phase spaces [2]. Although LBM has achieved great success for the simulation of many kinds of fluid flows such as MHD flows [3,4], very little research has been conducted for the lattice Boltzmann simulation of plasmas [5].

Many achievements of LBM development (especially multicomponent models [6–10]) can be inherited in the plasma simulation, since plasmas are mixtures of different types of particles. Among those models, the finite difference lattice Boltzmann (FDLB) models [7,8], can be used for the asymmetric system, which is the system in which the composite particles have different properties. However, the direct use of the FDLB models for plasma simulation is not sufficient due to some exclusive characteristics of plasmas. For example, in plasma simulation, the time step should be less than the electron oscillation period. If original plasma parameters are used, however, a very large nondimensional relaxation time will result. This relaxation time will significantly reduce the effects of the collision term on the evolution of the distribution function and thus lead to an ill-favored transport behavior of the electrons. Therefore, to overcome this, a relaxation time that is more suitable to the LBM must be obtained.

In this paper, to resolve the aforementioned problem, a rescaling scheme for the Boltzmann transport equation is proposed, which can be used for weakly ionized isothermal plasmas. Also, due to the huge difference between the lattice speeds of electrons and heavier particles (ions and neutrals), a second-order interpolation scheme is employed to find the on-node values of the discretized distribution functions for heavier particles. The developed LBM has been used to simulate electrostatic behaviors of weakly ionized isothermal plasmas and the obtained results show good agreement with theoretical solutions.

II. MATHEMATICAL MODEL

In this paper, the following assumptions are used:

(1) Inelastic collisions, such as ionization and recombination, are not considered.

(2) The plasma is isothermal, but different species can have different temperatures.

(3) The plasma consists of electrons, neutrals, and singly ionized ions (three species):

The Boltzmann transport equation for plasmas is written as follows:

$$\frac{\partial f_s}{\partial t} + \mathbf{v}_s \cdot \nabla f_s + \mathbf{a}_s \cdot \nabla_{\mathbf{v}_s} f_s = \left(\frac{\delta f_s}{\delta t} \right)_{coll}. \tag{1}$$

The subscript s denotes the type of species and can take e, i, and n for electrons, ions, and neutrals, respectively. In this equation, $\mathbf{v}_s$ is the microscopic velocity, $f_s = f_s(\mathbf{x}, \mathbf{v}, t)$ is the number density distribution function, and $\mathbf{a}_s$ is the acceleration due to the Lorentz force, which is expressed as

$$\mathbf{a}_s = \frac{q_s \mathbf{E}}{m_s} \tag{2}$$

if electrostatic behaviors of plasmas are considered. Here, $\mathbf{E}$ is electric field, q_s is the charge of species s, and m_s is the mass of species s.

By only considering the binary collisions in the plasma and applying the similar splitting technique adopted for the binary gas mixture [6], the collision term for species s can be written as

$$\left(\frac{\delta f_s}{\delta t} \right)_{coll} = J^{se} + J^{si} + J^{sn}, \tag{3}$$

where J^{se}, J^{si}, and J^{sn} are the terms that represent the collisions with electrons, ions, and neutrals, respectively. It is well known that if the degree of ionization is very low (say

*Corresponding author. hski@msu.edu

1–3%), the elastic collisions with neutral particles is the dominant collision mechanism for all species. Therefore, J^{se} and J^{si} are negligible in the weakly ionized plasmas. For the collisions with neutral particles, the Bhatnagar-Gross-Krook (BGK) model is used, which assumes that the particles relax to their equilibrium states during the characteristic time period, which is called the relaxation time λ_s. Then, the Boltzmann equations for electrons, ions, and neutrals can be written as

$$\frac{\partial f_e}{\partial t} + \mathbf{v}_e \cdot \nabla f_e + \mathbf{a}_e \cdot \nabla_{\mathbf{v}_e} f_e = -\frac{f_e - f_{en}^{eq}}{\lambda_{en}}, \tag{4}$$

$$\frac{\partial f_i}{\partial t} + \mathbf{v}_i \cdot \nabla f_i + \mathbf{a}_i \cdot \nabla_{\mathbf{v}_i} f_i = -\frac{f_i - f_{in}^{eq}}{\lambda_{in}}, \tag{5}$$

$$\frac{\partial f_n}{\partial t} + \mathbf{v}_n \cdot \nabla f_n = -\frac{f_n - f_{nn}^{eq}}{\lambda_{nn}}, \tag{6}$$

where λ_{en}, λ_{in}, and λ_{nn} are the relaxation times for electron-neutral, ion-neutral, and neutral-neutral collisions, respectively; f_{en}^{eq}, f_{in}^{eq}, and f_{nn}^{eq} are the equilibrium distribution functions of electrons, ions, and neutrals, respectively, due to the collisions with neutrals and can be written as

$$f_{sn}^{eq}(\mathbf{u}_{sn}) = \frac{n_s}{2\pi\theta_s^2} \exp\left(-\frac{(\mathbf{v}_s - \mathbf{u}_{sn})^2}{2\theta_s^2}\right). \tag{7}$$

Note that the collisions with the species other than neutral particles can be easily added in the model. In Eq. (7), $\theta_s = \sqrt{k_B T_s / m_s}$ is the sound speed of species s (where k_B is the Boltzmann constant and T_s is the temperature of species s); $\mathbf{u}_{sn}$ is the barycentric velocity of the binary collision with the neutral particle as follows:

$$\mathbf{u}_{sn} = \frac{\rho_s \mathbf{u}_s + \rho_n \mathbf{u}_n}{\rho_s + \rho_n}, \tag{8}$$

where $\mathbf{u}_s$ is the macroscopic velocity of species s ($\mathbf{u}_n$: macroscopic velocity of neutrals); ρ_s is the mass density of species s (ρ_n: density of neutrals). Note that $\mathbf{u}_{nn}=\mathbf{u}_n$, but $\mathbf{u}_{en} \neq \mathbf{u}_e$ and $\mathbf{u}_{in} \neq \mathbf{u}_i$. That is due to the fact that the frequency of self-collisions between charged particles is very low in weakly ionized plasmas and the charged particles cannot relax to their macroscopic velocity during the relaxation time period (λ_{en} or λ_{in}) when they collide with neutral particles.

Similar to the concept of density dependent relaxation time [11], λ_{sn} in Eqs. (4)–(6) are written as [12]

$$\lambda_{sn} = \frac{1}{\sigma_{sn} n_n \langle \bar{v}_s \rangle}. \tag{9}$$

Here, σ_{sn} is the cross section of the elastic collision between species s and neutrals and calculated as $\sigma_{sn}=\pi(r_s+r_n)^2$, where r_s and r_n are the radii of species s and n, respectively; $\langle \bar{v}_s \rangle$ is the average speed of species s, and $\langle \bar{v}_s \rangle = [(8/\pi)(k_B T_s/m)]^{1/2}$ [12]. Note that the relaxation time presented in Eq. (9) is independent of temperature because only isothermal plasmas are considered in this study.

One important point to note at this point is that electron temperature is too high to use the standard LBM even for low-temperature plasmas. For example, electron sound speed θ_e at $T_e=0.8$ eV is 3.75×10^5 m/s, which is extremely large considering the fact that the speed of sound in the LBM should be in the order of one [13]. Therefore, to overcome this problem, we choose the electron sound speed as follows:

$$\tilde{\theta}_e = \left(\frac{k_B T_e}{\tilde{m}_e}\right)^{1/2} = 1. \tag{10}$$

Here, tilde notation is used for rescaled variables. To satisfy Eq. (10) without changing temperature, the rescaled mass of electron should be obtained from Eq. (10) ($\tilde{m}_e = k_B T_e$, unit not correct), which is extremely large compared to the actual mass of electron. In addition to that, we propose the following rules to rescale other variables:

(1) The charge or mass ratio of electron is invariable: $e/m_e = \tilde{e}/\tilde{m}_e$.

(2) The mass ratio of different species is invariable: $m_e/m_i = \tilde{m}_e/\tilde{m}_i$ and $m_e/m_n = \tilde{m}_e/\tilde{m}_n$.

(3) Mass density of each species is invariable: $m_e n_e = \tilde{m}_e \tilde{n}_e$, $m_i n_i = \tilde{m}_i \tilde{n}_i$, and $m_n n_n = \tilde{m}_n \tilde{n}_n$.

(4) For the relaxation time rescaling, the time required to relax velocity is proportional to the magnitude of the velocity.

If we define $\gamma = \theta_e/\tilde{\theta}_e$ (where $\theta_e = \sqrt{k_B T_e/m_e}$ and $\tilde{\theta}_e = \sqrt{k_B T_e/\tilde{m}_e} = 1$), other variables are rescaled based on these rules in terms of γ. The relations between the original variables and rescaled variables are listed in Table I. From the fourth rule, the relaxation time is rescaled as $\tilde{\lambda}_{en} = (1/\gamma)\lambda_{en}$ since velocity is rescaled as $1/\gamma$. Note that in this rescaling scheme, time scale (other than relaxation time) is unchanged but length scale (both domain size and grid spacing) is squeezed by a factor of $1/\gamma$, which is different from the concept of superparticle used in the particle-in-cell (PIC) method [14] for plasmas, where a superparticle is regarded as a finite-sized cloud of real particles and both time and space scales are unchanged. In the present approach, however, all variables are rescaled using the rules before the LBM simulation, and the same rules are used again to recover original variables after the LBM simulation is completed. For the following discretization procedure, it is assumed that the rescaling is used and tilde notation will be dropped.

TABLE I. Relation between original parameters and modified parameters.

Parameter	Scaling
Mass of species s	$\tilde{m}_s = \gamma^2 m_s$
Number density of species s	$\tilde{n}_s = n_s/\gamma^2$
Unit charge	$\tilde{e} = \gamma^2 e$
Time step	$\delta\tilde{t} = \delta t$
Grid spacing, domain size ($\delta\tilde{x} = \sqrt{3}\tilde{\theta}_e \delta\tilde{t}$)	$\delta\tilde{x} = \delta x/\gamma$, $\tilde{l} = l/\gamma$
Relaxation time	$\tilde{\lambda}_{sn} = \lambda_{sn}/\gamma$

Now Eqs. (4)–(6) can be discretized using the standard LBM procedure. The forcing terms in Eqs. (4) and (5) are evaluated as follows [15,16]:

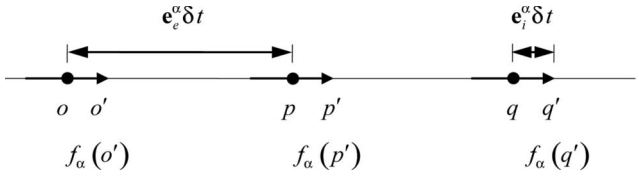

FIG. 1. Schematic of the second-order interpolation method for ion (neutral) distribution function.

$$\mathbf{a}_s \cdot \nabla_{\mathbf{v}_s} f_s \approx \mathbf{a}_s \cdot \nabla_{\mathbf{v}_s} f_s^{eq} = -\frac{\mathbf{a}_s \cdot (\mathbf{v}_s - \mathbf{u}_s)}{\theta_s^2} f_s^{eq}, \tag{11}$$

where f_s^{eq} is the equilibrium distribution function of species s due to self-collision.

$$f_s^{eq}(\mathbf{u}_s) = \frac{n_s}{2\pi\theta_s^2} \exp\left(-\frac{(\mathbf{v}_s - \mathbf{u}_s)^2}{2\theta_s^2}\right). \tag{12}$$

Note that the self-collision equilibrium distribution function (SCEDF) is used here rather than the cross-collision equilibrium distribution function (CCEDF). This selection will be justified in the discussion section. Equations (4)–(6) can be discretized as follows [17]:

$$f_e^\alpha(\mathbf{x} + \mathbf{e}_e^\alpha \delta t, t + \delta t) = f_e^\alpha(\mathbf{x}, t) - \frac{1}{\tau_{en}}[f_e^\alpha(\mathbf{x}, t) - f_{en}^{eq,\alpha}(\mathbf{x}, t)] + \frac{\delta t \mathbf{a}_e \cdot (\mathbf{e}_e^\alpha - \mathbf{u}_e)}{\theta_e^2} f_e^{eq,\alpha}, \tag{13}$$

$$f_i^\alpha(\mathbf{x} + \mathbf{e}_i^\alpha \delta t, t + \delta t) = f_i^\alpha(\mathbf{x}, t) - \frac{1}{\tau_{in}}[f_i^\alpha(\mathbf{x}, t) - f_{in}^{eq,\alpha}(\mathbf{x}, t)] + \frac{\delta t \mathbf{a}_i \cdot (\mathbf{e}_i^\alpha - \mathbf{u}_i)}{\theta_i^2} f_i^{eq,\alpha}, \tag{14}$$

$$f_n^\alpha(\mathbf{x} + \mathbf{e}_n^\alpha \delta t, t + \delta t) = f_n^\alpha(\mathbf{x}, t) - \frac{1}{\tau_{nn}}[f_n^\alpha(\mathbf{x}, t) - f_{nn}^{eq,\alpha}(\mathbf{x}, t)], \tag{15}$$

where δt is the time step; τ_{en}, τ_{in}, τ_{nn} are dimensionless relaxation times; superscript α denotes the αth component in the phase space; and $\mathbf{e}_s^\alpha$ is the αth component of the discretized microscopic velocity of species s.

$$\mathbf{e}_s^\alpha = \begin{cases} (0,0), & \alpha = 0 \\ (\cos\varphi_\alpha, \sin\varphi_\alpha) c_{ls}, & \varphi_\alpha = (\alpha - 1)\pi/2, \quad \alpha = 1,2,3,4 \\ \sqrt{2}(\cos\varphi_\alpha, \sin\varphi_\alpha) c_{ls}, & \varphi_\alpha = (\alpha - 5)\pi/2 + \pi/4, \quad \alpha = 5,6,7,8, \end{cases} \tag{16}$$

where $c_{ls} = \sqrt{3}\theta_s$ is the lattice speed of species s. Note that in the implementation of the present model, it was assumed that the momentum of particles conserves at each collision [18,19] so that the time-implicit treatment of the external force term [17] can be avoided. The discretized equilibrium distribution function $f_{sn}^{eq,\alpha}$ is expressed as [17]

$$f_{sn}^{eq,\alpha} = w_\alpha n_s \left[1 + \frac{3(\mathbf{e}_s^\alpha \cdot \mathbf{u}_{sn})}{c_{ls}^2} + \frac{9(\mathbf{e}_s^\alpha \cdot \mathbf{u}_{sn})^2}{2c_{ls}^4} - \frac{3\mathbf{u}_{sn}^2}{2c_{ls}^2}\right], \tag{17}$$

where w_α is 4/9 for $\alpha = 0$, 1/9 for $\alpha = 1,2,3,4$, and 1/36 for $\alpha = 5,6,7,8$.

In the multicomponent LBM, if the same grid is used for all species the time steps for different species are all different because each time step is determined by $\delta t = \delta x / c_{ls}$. Using several different time steps is very undesirable for a number of reasons, so in this study we use a single time step based on the lattice speed of electrons. Then, during a time step δt, electrons travel a distance of $\mathbf{e}_e^\alpha \delta t$ to the neighboring node while ions and neutrals travel a distance of $\mathbf{e}_i^\alpha \delta t$ and $\mathbf{e}_n^\alpha \delta t$. Since the lattice speeds of ions and neutrals are significantly smaller than that of electrons, the travel distance of those heavy particles will be very small compared to the electron travel distance. As a result, if the same grid is used for all species, ions and neutrals cannot reach the same nodal point as the electrons do and an interpolation scheme [2,20–23] needs to be used for heavier particles. In this study, similar to the interpolation scheme used in [21,22], a second-order interpolation method is introduced to find the on-node values of the discretized distribution functions for ions and neutrals. In Fig. 1, q and o denote two neighboring nodes of p along the αth direction (pointing from o to p). The ions (neutrals) that are originally located at o, p, q arrive at o', p', q' after a streaming step. The distribution function at p can be obtained by using $f_s^\alpha(o')$, $f_s^\alpha(p')$, and $f_s^\alpha(q')$ (after-collision distribution functions at p' and q') as follows:

$$f_s^\alpha(p) = f_s^\alpha(p') - \frac{f_s^\alpha(q') - f_s^\alpha(o')}{2} \frac{|\mathbf{e}_i^\alpha|}{|\mathbf{e}_e^\alpha|} + \frac{f_s^\alpha(q') - 2f_s^\alpha(p') + f_s^\alpha(o')}{2} \frac{|\mathbf{e}_i^\alpha|^2}{|\mathbf{e}_e^\alpha|^2}. \tag{18}$$

If we define $\beta = |\mathbf{e}_i^\alpha| / |\mathbf{e}_e^\alpha| = \sqrt{T_i m_e / T_e m_i}$, we obtain

$$f_s^\alpha(p) = (1 - \beta) f_s^\alpha(p') - 0.5\beta(1 - \beta) f_s^\alpha(q') + 0.5\beta(1 + \beta) f_s^\alpha(o'). \tag{19}$$

Note that $f_s^\alpha(p) \approx f_s^\alpha(p')$ because β is very small.

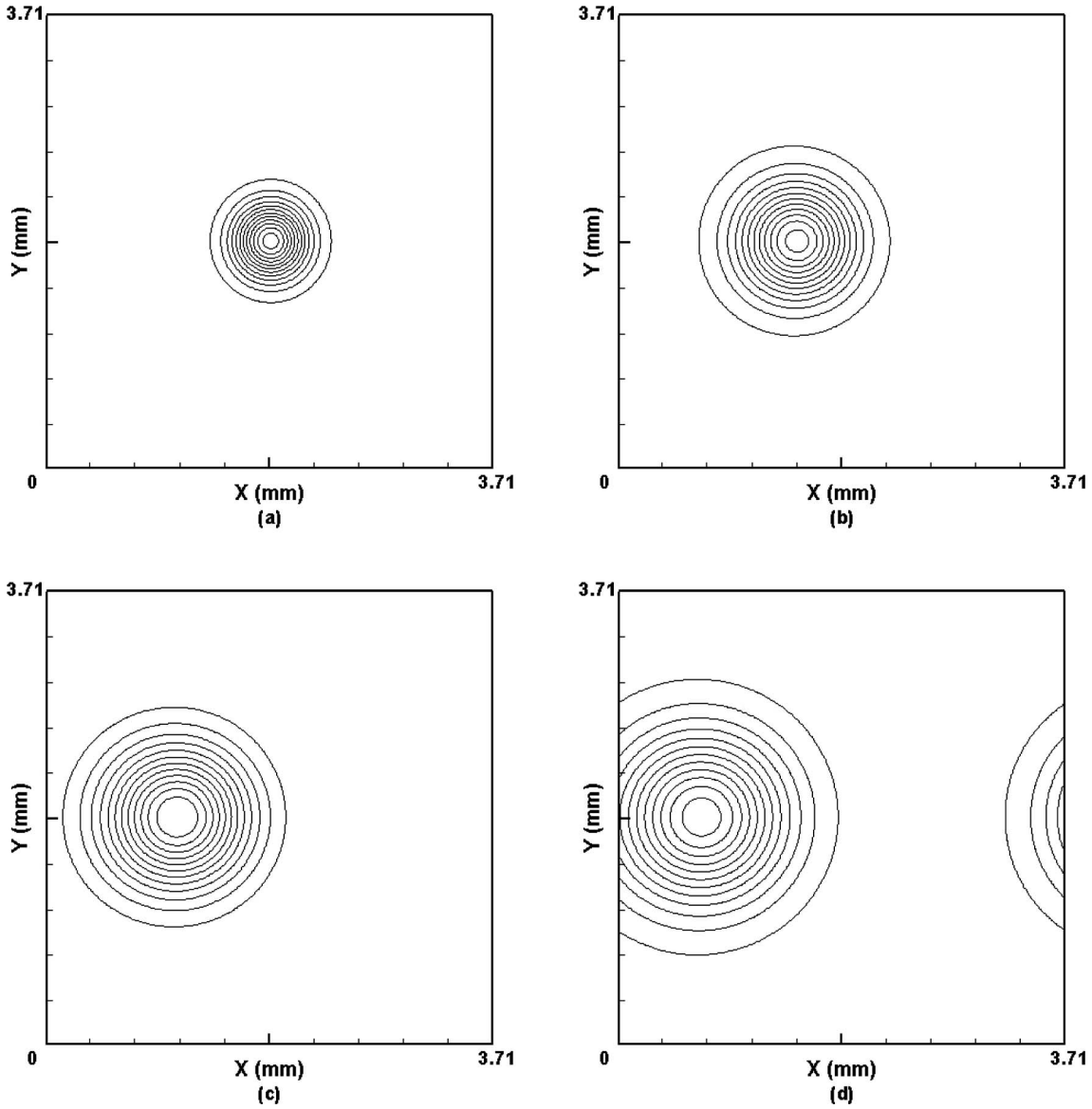

FIG. 2. Snapshots of the electron number density under an externally applied uniform electric field at (a) $t=0$ ns, (b) $t=3.35$ ns, (c) $t=6.70$ ns, and (d) $t=10.05$ ns (direction of E field: left→right).

Once distribution functions are updated, the number density and velocity of each species and charge density can be obtained as follows:

$$n_s(\mathbf{x}) = \sum_\alpha f_s^\alpha(\mathbf{x}), \tag{20}$$

$$n_s(\mathbf{x})\mathbf{u}_s(\mathbf{x}) = \sum_\alpha f_s^\alpha(\mathbf{x})\mathbf{e}_s^\alpha(\mathbf{x}), \tag{21}$$

$$\rho_v(\mathbf{x}) = e[n_i(\mathbf{x}) - n_e(\mathbf{x})]. \tag{22}$$

The electric field $\mathbf{E}$ is updated by solving the following equation:

$$\nabla^2\phi = -\frac{\rho_v}{\varepsilon_0}, \tag{23}$$

where ε_0 is the electric permittivity of the vacuum, ϕ is the electric potential, and $\nabla\phi=-\mathbf{E}$. Equation (23) is solved by a Poisson solver.

III. RESULTS

To validate the model, helium plasma with a 1% degree of ionization in a 3.71×3.71 mm domain (before rescaling) is considered, and a 256×256 grid is used. It is assumed that the temperature of electrons is 0.8008 eV and the temperature of ions and neutrals is 500 K. The corresponding number of densities of three species are $n_e=n_i=10^{16}$ (m^{-3}) and $n_n=10^{18}$ (m^{-3}) according to the Saha equation [12]:

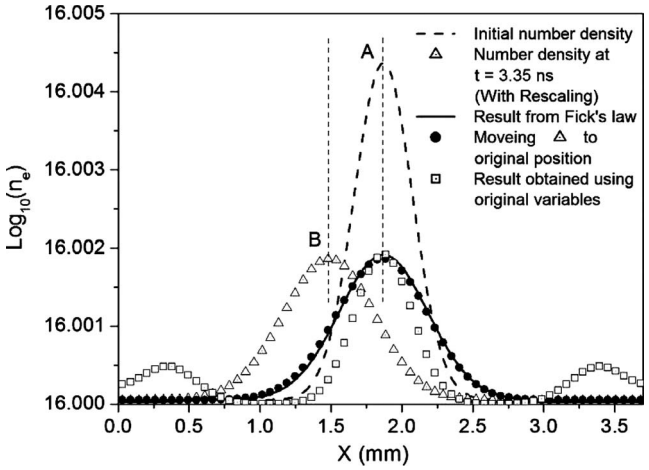

FIG. 3. Evolution of the electron number density under an externally applied uniform electric field (direction of E field: left $\rightarrow$right).

$$\frac{n_i}{n_n} \approx 3.00 \times 10^{27} T^{3/2} \frac{1}{n_i} \exp\left(-\frac{U}{T}\right), \tag{24}$$

where U is the first ionization energy of helium ($U=24.59$ eV) and T is the electron temperature in eV.

As the first validation, we consider the electron diffusion problem under an externally applied uniform electric field by neglecting the internally generated electric field (due to electrons and ions). In this case, the diffusivity (D) and drift velocity ($\mathbf{v}_d$) of the electrons can be obtained theoretically [24],

$$D = \frac{\langle \bar{v}_e \rangle^2 \lambda_{en}}{3}, \tag{25}$$

$$\mathbf{v}_d = -\frac{e\mathbf{E}_{ext}\lambda_{en}}{m_e}. \tag{26}$$

These theoretical results can be used to validate the model. The initial density distribution of electrons is assumed to be Gaussian as follows:

$$n_e(\mathbf{x}, t=0) = n_{e0}\left(1 + 0.01 \exp\left[-\frac{(x-x_c)^2 + (y-y_c)^2}{r^2}\right]\right), \tag{27}$$

where $r=0.290$ mm and (x_c, y_c) represents the center point of the domain. A uniform electric field of 0.025 V/m is applied in the positive x direction and the rescaling method is used. Figure 2 shows the snapshots of the evolution of the electron number density and Fig. 3 is the electron number density along the line of $y=y_c$. In Fig. 3, the initial number density profile (marked with A at the vertex) and the number density profile at 3.35 ns (marked with B at the vertex) are shown. As expected, electrons move in the opposite direction to the electric field and the drift velocity obtained from this simulation agrees very well with the theoretical value predicted by Eq. (26). The difference is about 0.843%. The plasmas with ionization degrees of 2% and 3% are also simulated under the same conditions as described above. Since the higher ionization degree is caused by a higher electron temperature, the sound speed of the electron is also higher and a smaller relaxation time λ_{en} results. Therefore, according to Eq. (26), the plasma with a higher ionization degree will show a smaller drift velocity. Errors in the drift velocity for 2% and 3% ionized plasmas are 0.86% and 0.87%, respectively, compared to Eq. (26).

In order to calculate the diffusivity from the simulation result, the curve (B) is moved to the initial location (small solid circles in Fig. 3) and is compared with the solution to Fick's law with the theoretical diffusivity D given in Eq. (25).

$$\frac{\partial n_e}{\partial t} = D\nabla^2 n_e. \tag{28}$$

It is apparent that the result obtained by the rescaling method agrees very well with Fick's law solution (solid line in Fig. 3).

We also simulated the problem without the rescaling and the results are shown as squares in Fig. 3 and also in Fig. 4. Clearly, without rescaling, the result is very inaccurate and nonphysical peaks appear in the solution. The appearance of these nonphysical peaks can be explained as follows. In the case of electrons, the large nondimensional relaxation time leads to a near-zero collision term in the lattice Boltzmann equation, and therefore, the effect of collision step is almost negligible. In other words, virtually only the streaming step is left in the implementation of LBM. This is evident from Fig. 4, where the subpeaks move with the constant lattice speeds and the magnitudes do not change. We can also see that the subpeaks of higher ionization degree move faster than those of lower ionization degree because the sound speed is higher in the former case. The magnitudes of all three subpeaks are also checked: the ratio of the magnitude of a subpeak to that of the primary peak is 1:4, which is the ratio of weight coefficients in the D2Q9 model employed in this study. Figure 5 is the contour plot of the electron number density at $t=1.116$ ns obtained without the rescaling. The dashed lines in the plot represent the discretized phase space and the particles stream to their neighboring nodes along the directions denoted by the numbers. The numbers in parentheses are the weight coefficients used in the discretization of the equilibrium distribution function. In Fig. 5, it seems as though the LBM simulation was conducted without the collision step. Therefore, the presented rescaling method not only recovers the correct transport phenomena but is also required in the simulation of weakly ionized plasmas.

One thing to recall at this point is the fact that the external force in the lattice Boltzmann equation [Eq. (11)] was evaluated by using SCEDF rather than CCEDF. To justify this we used both CCEDF and SCEDF for the same simulation and the results are shown in Fig. 6. Since it is a simple convection-diffusion problem, the ratio n_e/n_{e0} cannot be smaller than 1. However, it is seen that when CCDEF is used the number density away from the peak can take values smaller than the initial value. As shown in Fig. 6, the minimum value is roughly 0.9997, which means that the number

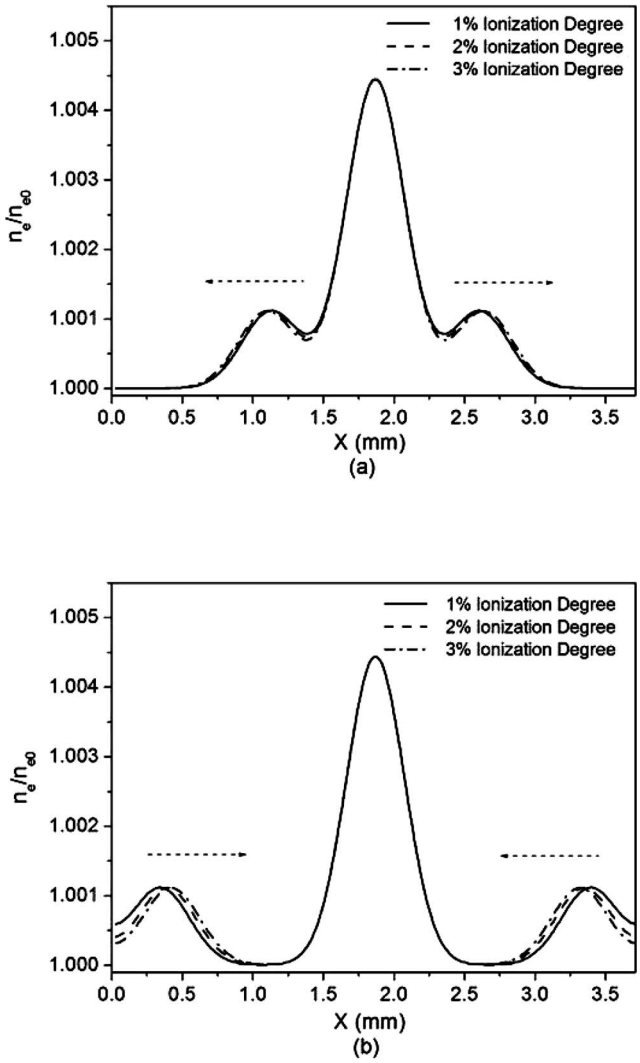

FIG. 4. Electron number density distribution at (a) $t=1.116$ ns and (b) $t=3.347$ ns (without the rescaling of variables).

density drops by about 3% of the initial perturbation of electron number density. On the other hand, physically realistic results were obtained with the use of SCEDF.

The grid independency and computational efficiency of the model are also studied by conducting the same simulation on three different grids (64×64, 128×128, and 256×256). The error at time t was calculated as follows:

$$\text{error} = \sqrt{\sum_{i,j}\left[\frac{n_e^{LB}(i,j,t)-n_e^{A}(x_i,y_j,t)}{n_e^{A}(x_i,y_j,t)}\right]^2} \Bigg/ mn, \quad (29)$$

where m and n are grid numbers in x and y directions, respectively; $n_e^{LB}(i,j,t)$ is the electron number density at node (i,j) obtained by the present model; and $n_e^{A}(x_i,y_j,t)$ represents the electron number density at the corresponding space point obtained from the following analytical solutions:

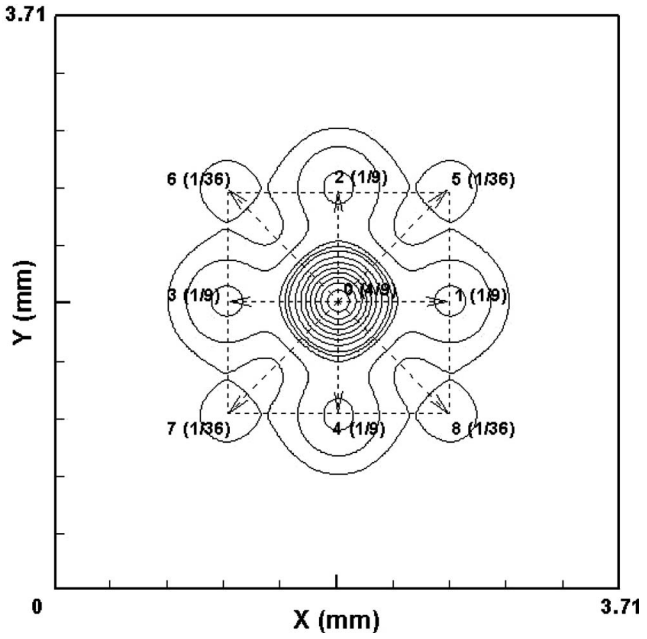

FIG. 5. Contour plot of the electron number density at $t=1.116$ ns (no rescaling is used).

$$n_e(x,y,t) = n_{e0} + \frac{0.01n_{e0}}{(1+t/t_0)}\exp\left[-\frac{(x-x_c)^2+(y-y_c)^2}{r^2(1+t/t_0)}\right], \quad (30)$$

where $t_0=r^2/4D$ and the diffusivity D can be calculated from Eq. (25). Figure 7 shows that, as expected, second-order convergence is observed from the simulation results.

In order to test the computational efficiency of the multicomponent model, CPU times per time step are measured on a single-CPU PC for the present three-component model with the interpolation and a simple LBE model for electrons only. The electrostatic equation is not considered in the test. Test results show that the three-component model takes 4.07 times more CPU time than the electron-only model.

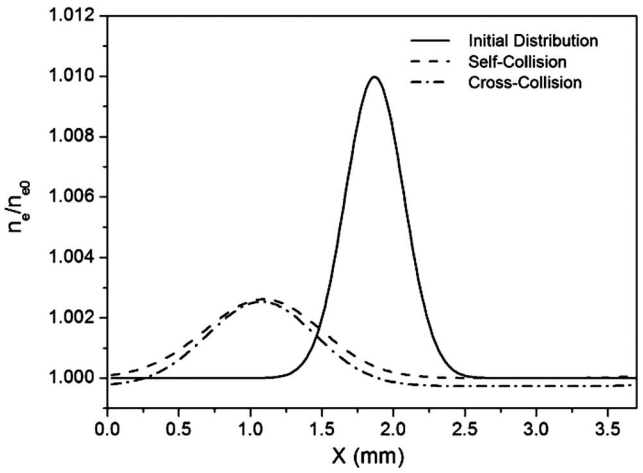

FIG. 6. Electron number density distribution (at $t=6.69$ ns) obtained by using different equilibrium distribution functions for the external force term.

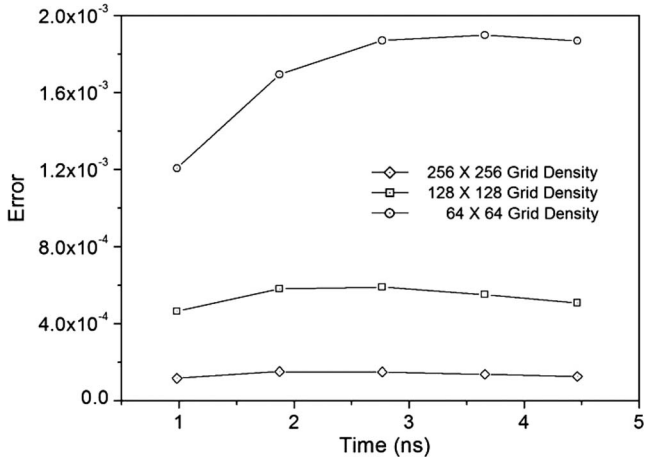

FIG. 7. Relative errors in the electron number density vs time for three different grids. The errors are calculated at the center of the domain with comparison to the analytical solution.

Figure 8 presents the effect of the internal electric field on the diffusion process. In this case, the external electrical field is not applied and only the internally generated electric field is considered during the diffusion process. It can be seen that the diffusion process is enhanced by the internally generated electric field.

As a second validation of the model, we consider the electrostatic wave problem by neglecting all collision terms in Eqs. (4)–(6). If the collision term in the Boltzmann equation is neglected, the Boltzmann equation becomes the Vlasov equation for collisionless plasmas. The initial spatial distribution of the electron number density is perturbed slightly as follows:

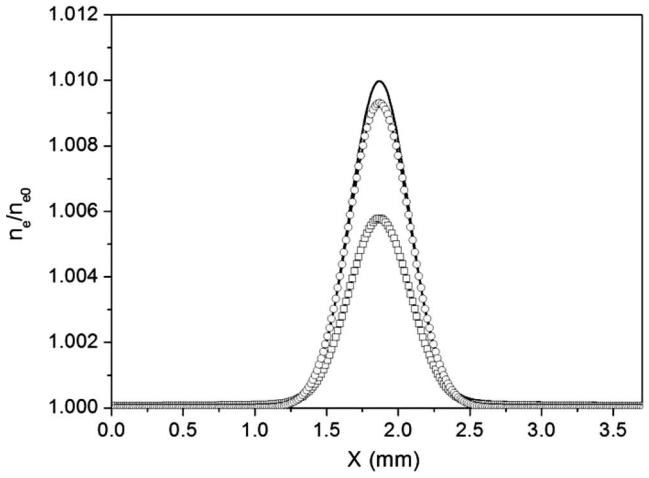

FIG. 8. Electron number density distribution. (Circle: without internal electric field; squares: with internal electric field, both at 0.223 ns. The solid line shows the initial distribution.)

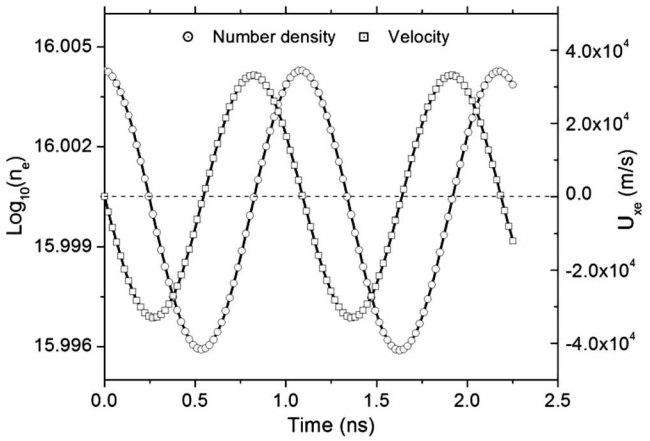

FIG. 9. Time evolution of number density and x-component velocity of electrons at the center of the computational domain. (Solid lines: simulation results obtained without the rescaling scheme; circles and squares: simulation results obtained with the rescaling scheme.)

$$n_e(\mathbf{x}, t=0) = n_{e0}\left[1 - 0.01\cos\left(\frac{2\pi x}{l_x}\right)\right], \tag{31}$$

where l_x is the length of the physical domain (3.71 mm). The periodic boundary condition is employed for both the streaming step for the LBM and the Poisson equation for the electric potential. For this problem, we used both with and without the rescaling. It is possible because all the collision terms are neglected. Figure 9 shows the evolution of electron number density and x-component velocity at the center point of the domain. It is clear that the results obtained with the rescaling scheme agree very well with the ones obtained using original variables. In addition, the wave period measured from the figure agrees well with the theoretical value of the electron oscillation period ($2\pi/\omega_{pe}$ [12]). The maximum relative error between the theoretical and simulation results is 0.22%. Therefore, both the standard LBM and the rescaled LBM can be used for the collisionless Vlasov equation.

IV. CONCLUSION

In summary, a lattice Boltzmann method for weakly ionized isothermal plasmas has been presented. A rescaling scheme has been presented to convert the relaxation time based on plasma physics to the proper relaxation time for LBM simulation, so that the effects of collisions are taken into account correctly in the LBM. To use a single time step based on electrons, an interpolation method has been employed for ions and neutrals. Simulation results agree well with theoretical predictions. Also, it has been shown that for a collisionless Vlasov equation the rescaling scheme need not be used.

ACKNOWLEDGMENTS

This research was supported, in part, by the National Science Foundation (Grant No. 0425217) and Michigan State University.

[1] S. Chen and G. D. Doolen, Annu. Rev. Fluid Mech. **30**, 329 (1998).
[2] X. Y. He and L. S. Luo, Phys. Rev. E **55**, R6333 (1997).
[3] S. Y. Chen, H. D. Chen, D. Martinez, and W. Matthaeus, Phys. Rev. Lett. **67**, 3776 (1991).
[4] D. O. Martinez, S. Y. Chen, and W. H. Matthaeus, Phys. Plasmas **1**, 1850 (1994).
[5] A. I. D. Macnab, G. Vahala, L. Vahala, J. Carter, M. Soe, and W. Dorland, Physica A **362**, 48 (2006).
[6] L. S. Luo and S. S. Girimaji, Phys. Rev. E **66**, 035301 (2002).
[7] Z. L. Guo and T. S. Zhao, Phys. Rev. E **71**, 026701 (2005).
[8] A. G. Xu, Phys. Rev. E **71**, 066706 (2005).
[9] V. Sofonea and R. F. Sekerka, Physica A **299**, 494 (2001).
[10] P. Asinari, Phys. Rev. E **73**, 056705 (2006).
[11] V. Sofonea and R. F. Sekerka, Phys. Rev. E **71**, 066709 (2005).
[12] J. A. Bittencourt, *Fundamentals of Plasma Physics* (Springer, New York, 2004).
[13] S. Succi, *The Lattice Boltzmann Equation for Fluid Dynamics and Beyond* (Clarendon Press, Oxford/Oxford University Press, New York, 2001).
[14] R. W. Hockney and J. W. Eastwood, *Computer Simulation using Particles* (A. Hilger, Bristol, England/Philadelphia, 1988).
[15] R. R. Nourgaliev, T. N. Dinh, T. G. Theofanous, and D. Joseph, Int. J. Multiphase Flow **29**, 117 (2003).
[16] X. Y. He, X. W. Shan, and G. D. Doolen, Phys. Rev. E **57**, R13 (1998).
[17] X. Y. He and L. S. Luo, Phys. Rev. E **56**, 6811 (1997).
[18] A. K. Gunstensen, D. H. Rothman, S. Zaleski, and G. Zanetti, Phys. Rev. A **43**, 4320 (1991).
[19] D. Grunau, S. Y. Chen, and K. Eggert, Phys. Fluids A **5**, 2557 (1993).
[20] X. Y. He, L. S. Luo, and M. Dembo, J. Comput. Phys. **129**, 357 (1996).
[21] Z. L. Guo, C. G. Zheng, and T. S. Zhao, J. Sci. Comput. **16**, 569 (2001).
[22] X. Y. He and G. D. Doolen, Phys. Rev. E **56**, 434 (1997).
[23] X. Y. He, L. S. Luo, and M. Dembo, Physica A **239**, 276 (1997).
[24] T. Makabe, *Plasma Electronics: Applications in Microelectronic Device Fabrication* (CRC Press, Hoboken, 2006).